SLAC-PUB-10481

TAKING X-RAY DIFFRACTION TO THE LIMIT: Macromolecular Structures from Femtosecond X-Ray Pulses and Diffraction Microscopy of Cells with Synchrotron Radiation*

Jianwei Miao,[1] Henry N. Chapman,[2] Janos Kirz,[3] David Sayre,[3] and Keith O. Hodgson[1,4]

[1]*Stanford Synchrotron Radiation Laboratory, Stanford Linear Accelerator Center, Stanford University, Stanford, California 94309-0210; email: miao@ssrl.slac.stanford.edu; hodgson@ssrl.slac.stanford.edu*

[2]*Lawrence Livermore National Laboratory, Livermore, California 94550; email: chapman9@llnl.gov*

[3]*Department of Physics and Astronomy, Stony Brook University, Stony Brook, New York 11794; email: kirz@xray1.physics.sunysb.edu; sayre@xray1.physics.sunysb.edu*

[4]*Department of Chemistry, Stanford University, Stanford, California 94305*

Key Words oversampling phasing method, iterative algorithms, diffraction microscopy, X-ray free electron lasers, single molecule imaging

■ **Abstract** Recent work is extending the methodology of X-ray crystallography to the structure determination of noncrystalline specimens. The phase problem is solved using the oversampling method, which takes advantage of "continuous" diffraction patterns from noncrystalline specimens. Here we review the principle of this newly developed technique and discuss the ongoing experiments of imaging nonperiodic objects, such as cells and cellular structures, using coherent and bright X rays produced by third-generation synchrotron sources. In the longer run, the technique may be applicable to image single biomolecules using anticipated X-ray free electron lasers. Here, computer simulations have so far demonstrated two important steps: (*a*) by using an extremely intense femtosecond X-ray pulse, a diffraction pattern can be recorded from a macromolecule before radiation damage manifests itself; and (*b*) the phase information can be retrieved in an ab initio fashion from a set of calculated noisy diffraction patterns of single protein molecules.

Submitted to Annu. Rev. Biophys. Biomol. Struct. 2004

Work supported by Department of Energy contract DE-AC03-76SF00515.

.

CONTENTS

PERSPECTIVE AND OVERVIEW

X-ray crystallography yields high-resolution three-dimensional images of molecules in the crystalline state and provides essential information in many areas of biology today. However, in important areas of molecular biology and throughout cell biology, structures of key biological interest exist which cannot currently be crystallized and hence are not accessible by conventional crystallography. An effort has therefore been underway for some years to extend the diffraction methodology employed in X-ray crystallography to the general small noncrystalline specimen, the extended methodology we refer to as X-ray diffraction microscopy. This approach, based primarily on the emergence of more powerful synchrotron X-ray sources and on the presence of more favorable circumstances for dealing with the phase problem, is now looking promising and is the subject of this review.

"General small specimen" refers to a nonperiodic isolated object of less than a few microns in size. This definition encompasses such species as a single biomolecule, a macromolecular assembly, an organelle, or a complete small cell. (Larger and nonisolated objects are additional possibilities for the future.) The objects covered closely resemble the objects covered by optical and electron microscopy. But X-ray diffraction microscopy offers imaging resolution that is much higher than that possible with the optical microscope and allows specimen thickness much higher than in the electron microscope.

In comparing diffraction microscopy with crystallographic imaging, the main difference is that the intensity of the diffraction signal is much weaker in the noncrystalline case. This is due to the absence of the large signal amplification that occurs at the Bragg peaks in the crystal case; that amplification can be of the order of N^2, where N is the number of unit cells in the crystal. This lowering of signal explains why the development of new X-ray sources is important for diffraction microscopy—we are asking for the increase in source brightness to compensate for the loss of Bragg-peak amplification. Fortunately, new sources of

synchrotron radiation appear capable of living up to that request. Equally important is a second condition, namely, that the specimen used in diffraction microscopy be capable of withstanding a greatly intensified X-ray exposure. As will be seen, this will, at least in the field of biological specimens, set the resolution limit of the technique.

The absence of Bragg-peak amplification also has an advantage; the observed diffraction pattern does not lose the information that exists between the Bragg peaks. The favorable consequence of this is that the phase problem, difficult for crystals, becomes simpler for diffraction microscopy. While more experience will be needed, as described below, indications are that phasing will not be a central problem for this type of imaging (see The Oversampling Phasing Method and Iterative Algorithms, below).

Returning to the problem of specimens withstanding increased radiation exposure, there are two basic cases to consider. In the first case the sample is noncrystalline, but there exists a large supply of exact copies of the structure of interest, whereas in the second case, exact copies do not exist. The first case is exemplified by a protein molecule and is the more favorable in terms of the high-resolution quality of three-dimensional imaging that can be envisioned; the second case is exemplified by a whole biological cell. In the first case, a femtosecond flash X-ray source can be used to capture diffraction data before the damage has had time to become evident, with many copies of the structure required for collection of the full three-dimensional dataset. In the second case the strategy must be to employ approaches such as cryoprotection to extend the lifetime of the specimen as much as possible during the three-dimensional data collection in a high-brightness synchrotron X-ray beam. Detailed simulations indicate that in the first scenario, near-atomic-resolution imaging is possible at least for relatively large macromolecules, whereas for the second scenario, 10 nm (or large-molecular) resolution may be possible. The first and second cases are discussed in detail below (see From Storage-Ring-Based to Linac-Based X-Ray Sources, Overcoming the Radiation Barrier with Femtosecond X-Ray Pulses, and Potential of Imaging Single Protein Molecules, below).

Historically, work in this area began in the early 1980s at the Stony Brook physics department and the Brookhaven synchrotron (59). By 1990 it was established (76, 60) that the diffraction pattern can be recorded from general small specimens using synchrotron radiation. In 1995, an approximate treatment was given (61) of the relationship between dose and resolution, and by 1998 it was established (49, 60, 62) that the gain of information between Bragg peaks greatly enhances the solvability of the phase problem. Finally, in 1999 Miao et al. (42) successfully demonstrated the complete procedure of pattern recording, phasing, and imaging for a two-dimensional man-made radiation-resistant specimen. Subsequent to these developments, other groups began to take up the subject (see references in later sections), and with these efforts considerable research strength in the field has now been added.

THE OVERSAMPLING PHASING METHOD AND ITERATIVE ALGORITHMS

The Principle of the Oversampling Method

The discovery of X-ray diffraction from crystals by von Laue in 1912 marked the beginning of a new era for visualizing the three-dimensional atomic structures inside crystals. Indeed, after almost a century's development, X-ray crystallography has developed to a point where it can determine almost any structure, as long as good-quality crystals are obtained. This remarkable achievement can be partially attributed to the development of powerful crystallographic phasing methods such as the direct methods (20), isomorphous replacement (21), molecular replacement (1), multiple wavelength anomalous dispersion (26, 54), and others (75). However, when the crystals become small or have only one unit cell (i.e., noncrystalline), the X-ray diffraction intensities are weak and continuous, and the crystallographic phasing methods can be improved upon. When the diffraction pattern is continuous, the phase information is much easier to recover by sampling the diffraction pattern at a spacing finer than the Bragg-peak frequency (i.e., oversampling). It was first suggested by Sayre (58) in 1952 that knowledge of the intensities between, as well as at, the Bragg peaks may provide the phase information. Bates (4) proposed an explanation for the oversampling method in 1982. On the basis of the argument that the autocorrelation function of any sort of object is twice the size of the object itself in each dimension, Bates concluded that the phase information could be recovered only by sampling the intensities in each dimension twice finer than the Bragg-peak frequency. In 1996, Millane (50) further extended Bates' criterion to three and higher dimensions.

In 1998, Miao et al. (49) proposed a different explanation for the oversampling method and concluded that Bates' criterion is overly restrictive. If each intensity point is considered a nonlinear equation (which is related to the electron density in the specimen by the square of the magnitude of the Fourier transform), the solution to the phase problem becomes the problem of solving this set of equations to recover the unknown electron density. When the intensities are sampled at Bragg-peak frequency, there are exactly twice as many unknowns as independent equations (48), where independent equations are defined as those intensity points having no crystallographic symmetry relationship. This is why, in the absence of any other information, phases cannot be directly recovered from the diffraction pattern sampled at Bragg-peak frequency. When the diffraction pattern is sampled at a spacing finer than the Bragg-peak frequency, the number of independent equations increases while the number of unknown variables remains the same.

Oversampling of the diffraction pattern requires better coherence of the incident X rays than does Bragg sampling. The illumination needs to be both temporally (narrow bandwidth) and spatially (tight collimation) coherent (45, 46). This is because the higher oversampling frequencies require finer recording of the features in the diffraction pattern. Equivalently, oversampling the diffraction pattern

corresponds to surrounding the electron density with a no-density region, where the size of the no-density region is proportional to sampling frequency (48). An oversampling ratio was introduced to characterize the oversampling degree, which is defined as the ratio of the volume of the electron density and no-density region to the volume of the electron density region (49). When the ratio is larger than 2, the number of independent equations is more than the number of unknown variables, and the phase information is in principle embedded inside the diffraction pattern. Having a larger number of independent equations than unknowns is a necessary, but not sufficient, condition to guarantee a unique solution. From the theory of polynomials, given a noise-free diffraction pattern, there are usually $\leq 2^M$ multiple solutions in one dimension, where M is the number of unknown variables (2, 11). In two and three dimensions, the multiple solutions are rare because two- and three-dimensional polynomials usually cannot be factorized.

Iterative Algorithms

Although in principle there exists a unique phase solution in an oversampled two- or three-dimensional diffraction pattern with an oversampling ratio greater than 2, it is not straightforward to find the solution (i.e., global minimum) from the large number of nonlinear equations. One of the most effective ways to accomplish this is to use iterative algorithms. In 1972, Gerchberg & Saxton (19) proposed a phase retrieval algorithm by iterating back and forth between real and reciprocal space. An electron micrograph and an associated diffraction pattern can be used as constraints in real and reciprocal space, respectively. In 1978, Fienup (16) further improved the iterative algorithm by using the finite size of an object (termed the support, or mask) and positivity as constraints in real space, where the positivity constraint is due to the fact that the electron density should be positive. Independently, Stroud & Agard (68) developed an iterative Fourier method in 1979 for the phase retrieval and refinement of the continuous one-dimensional diffraction pattern of membranes. Although oversampling of continuous intensities in one dimension usually has multiple phase solutions, a unique solution may be obtained under certain conditions. In subsequent years, the shape of the finite support was thought to be critical to phasing two- and three-dimensional diffraction patterns (16, 17). However, both simulation and experimental results suggested that the oversampling ratio is one of the deterministic factors to the success of phase retrieval (45, 49). Recently, Elser (15) introduced a different algorithm for iterative phase retrieval, which he refers to as the difference map approach. In model calculations it is particularly powerful when the support constraint is poorly known and when there is additional information about the specimen, such as atomicity or the spectrum of scattering strengths present in the form of a histogram. The iterative phase retrieval of complex-valued objects has also been pursued. By using tight support (17), enforcing positivity on the imaginary part of the objects (49), or applying more constraints such as histogram profiles (33), correct phase information can usually be retrieved.

Iterative algorithms have now reached a point in which phase information can usually be reliably recovered from an oversampled diffraction pattern with reasonable signal-to-noise ratio. These algorithms, based on the Fienup approach (16), usually consist of the following four steps in each iteration (45).

1. The magnitude of Fourier transform (i.e., square root of the measured diffraction intensities) is combined with the current best phase set. A random phase set is used for the first iteration.
2. Applying the inverse fast Fourier transform, a new electron density function is obtained.
3. Constraints are enforced on the electron density function. By pushing the electron density outside the support and the negative electron density inside the support close to zero, and retaining the positive electron density inside the support, a new electron density is defined.
4. Applying the fast Fourier transform to the new electron density, a new set of phases is calculated. After setting the phase of central pixel to zero, this new phase set is used for the next iteration.

Note that there are other algorithms under development that, although iterative, do not involve cycles of forward and inverse transforms. These efforts are extensions of methods used in crystallography, helped by the fact that they can incorporate oversampled data. The first involves an application of direct methods (67), and the second is a real-space conjugate-gradient minimization based on the EDEN program (S.P. Hau-Riege, H. Szöke, H.N. Chapman & A. Szöke, manuscript submitted).

The combination of the oversampling method with iterative algorithms is gradually becoming a general and powerful phasing technique. It does not require atomic resolution of the diffraction pattern and can solve large and complicated structures. Although bearing some relationship to solvent flattering (71), noncrystallographic symmetry (10, 13, 57) and molecular replacement (1), the oversampling method does not need crystal samples and is an ab initio phase method. The generality of the oversampling method is due to the fact that the no-density region can be determined in an ab initio fashion, and the size of the no-density region is proportional to the sampling frequency. However, the major drawback to this approach is that the diffraction intensities are relatively weak. To carry out these experiments, it is necessary to use bright X-ray sources such as the third-generation synchrotron sources; for imaging single biomolecules, future X-ray free electron lasers (XFELs) will be required.

EXPERIMENTS USING SYNCHROTRON RADIATION

The possible extension of the methodology of X-ray crystallography to noncrystalline specimens (i.e., X-ray diffraction microscopy) was first suggested by Sayre in 1980 (59). While the concept is simple and elegant, the experiment itself is

challenging in that the loss of crystallinity makes it difficult to record a high-quality diffraction pattern. In subsequent years, progress has been made in recording diffraction patterns from noncrystalline specimens (62, 76). However, it was not until 1999 that the first demonstration experiment was carried out by Miao et al. (42). Figure 1*a* shows a test pattern made of a patch of Au dots on a silicon nitride membrane. The specimen was illuminated by coherent X rays with a wavelength of 17 Å. Figure 1*b* shows an oversampled diffraction pattern (450 × 450 pixels), with the oversampling ratio equal to 25. Due to the presence of a beamstop to block the direct beam, there were missing data in a 15-pixel-radius circle at the center, which were filled in by the intensities calculated from a lower-resolution X-ray microscopy image (31). By using the iterative algorithm, the unique phase information was successfully retrieved, as shown in Figure 1*c*. Since that demonstration, X-ray diffraction microscopy has been successfully applied to imaging a series of noncrystalline specimens and nanocrystals (23, 37, 41, 45, 47, 56, 66, 70, 73), in some cases even without the need to patch in missing data due to the beamstop. The three-dimensional imaging of noncrystalline specimens using the oversampling phasing method has also been demonstrated recently, requiring the recording of a number of two-dimensional diffraction patterns by rotating the specimen about one axis (46, 74).

The application to biological samples has also been pursued (43) to study *Escherichia coli* bacteria with manganese labeling of histidine-tagged yellow fluorescent proteins. The bacteria were air-dried and supported on a silicon nitride window. Using coherent X rays with a wavelength of 2 Å from an undulator beamline at SPring-8, an oversampled diffraction pattern was recorded, as shown in Figure 2*a*. The intensities in an area of 70 × 70 pixels at the center of the pattern were filled in by a patch of data calculated from a lower-resolution X-ray micrograph. This oversampled diffraction pattern was directly converted to an image with a resolution of ∼30 nm (Figure 2*b*). The reconstructed bacteria contain dense regions that probably represent the histidine-tagged proteins labeled with manganese, with a semitransparent region that is devoid of proteins. These observations were confirmed by both transmission and fluorescence microscopy images shown in Figure 2*c*.

Looking forward, this methodology can in principle be applied to imaging whole cells and cellular structures in three dimensions, which are too thick for electron microscopy (5, 40). The resolution will likely be limited by radiation damage (25, 36, 63; see also Overcoming the Radiation Barrier with Femtosecond X-ray Pulses, below). By cooling samples down to liquid nitrogen or even liquid helium temperatures, previous X-ray experiments have shown that the radiation damage problem can be greatly reduced (38, 64). Indeed, the Stony Brook group has already embarked on the task of creating a three-dimensional image of the yeast *Saccharomyces cerevisiae*. Because this task involves the collection of hundreds of diffraction patterns as the specimen is rotated, a special instrument was built for this purpose (7). It incorporates a cryo-holder, so that the frozen hydrated specimen can be kept at liquid nitrogen temperatures to minimize radiation damage. It also incorporates computer-controlled motorized stages to automate the

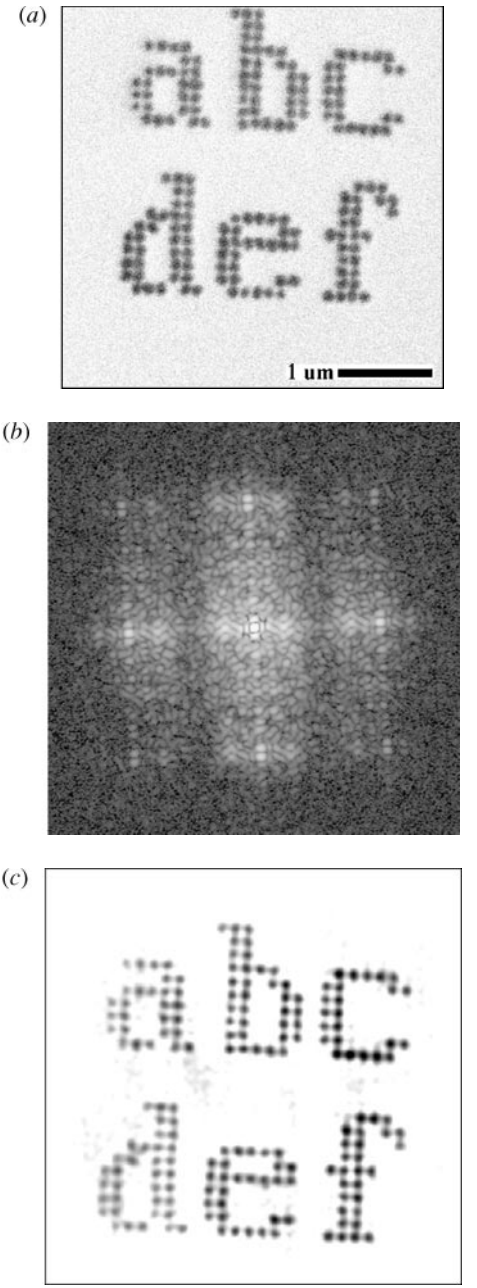

Figure 1 Phase retrieval of an oversampled diffraction pattern recorded from a non-crystalline specimen. (*a*) A scanning electron microscopy image of the specimen. (*b*) An oversampled X-ray diffraction pattern of the specimen. (*c*) A specimen image as directly reconstructed from (*b*). (See Reference 42 for details.)

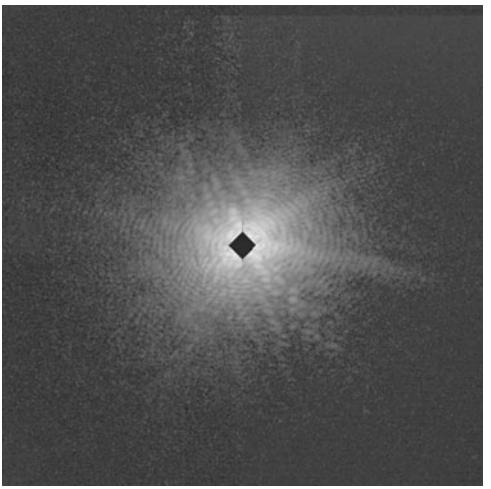

Figure 3 An X-ray diffraction pattern from the yeast *S. cerevisiae*. The pattern is a composite of several exposures and displays the square root of the recorded diffraction intensity on a semilog scale.

alignment and rotation. Figure 3 shows the diffraction pattern of a freeze-dried yeast cell obtained at the National Synchrotron Light Source, where this instrument was used. Because the experiment is highly demanding of coherent flux, data collection for three-dimensional imaging requires the brightest sources of soft X rays currently available, among those being the Lawrence Berkeley Laboratory's Advanced Light Source.

FROM STORAGE-RING-BASED TO LINAC-BASED X-RAY SOURCES

Intense synchrotron sources play a key role in current and future diffraction microscopy experiments. The use of synchrotron radiation produced by electron storage rings was recognized and had begun to be exploited in the 1970s. Indeed, among the earliest and most dramatic demonstrations of the value of this intense source of radiation were experiments carried out at Stanford on protein diffraction that clearly showed the value of both the high intensity (to obtain higher-resolution diffraction patterns in much shorter time) (55) and the prospects for the use of anomalous dispersion to solve the phase problem (which has come to be known as MAD phasing) (54). Although these early studies showed significant promise, it took more than a decade for synchrotron radiation to come into more routine use for macromolecular crystallography as well as biological small-angle and X-ray absorption studies. This was due in part to the sources themselves (in particular,

their unreliable operation early in their history) as well as the instrumentation available at that time (e.g., no electronic data-recording media for diffraction patterns). The early generation of storage rings was initially derived from those used for high-energy physics (first generation) and evolved and became more optimized for synchrotron radiation production (second generation). As the sources themselves became much more reliable, and effective instrumentation was developed for taking measurements, there began a strong movement toward using synchrotron radiation for X-ray-based studies in structural biology (72). Consequently, since the 1980s and into the 1990s, the most challenging structural biology problems were often addressed using synchrotron X rays.

In the 1990s, a new class of synchrotron sources began to come online. These machines, called third-generation sources, had lattices that were optimized for accepting insertion devices called undulators. Undulators are one class of devices developed to be located in straight sections where synchrotron radiation would not normally be produced. The most common class of insertion device used early on (in the late 1970s) was called a wiggler. Wigglers can have locally higher fields that alternately bend the path of the electron beam back and forth, shifting the critical energy higher (and hence making the radiation "harder") and increasing intensity by a simple incoherent addition of the radiation from each of the bends (by a factor of N, the number of poles). Wigglers have been constructed and operated with high fields (superconducting) or moderate fields (electromagnet or permanent magnet), and there are a variety of configurations with different numbers of poles (from a few to 50 or more) in use at many synchrotrons around the world. By using weaker fields and defining a phase relationship between the radiation emitted from one pole to the next, another class of insertion devices was developed, in this case built primarily from relatively weak field permanent magnet arrays (such as SmCo or NdFeB).

Undulators provide a much narrower opening angle of radiation, in which constructive interference effects dramatically increase the delivered beam brightness (where in contrast to wigglers, the gain scales as N^2). They can also be readily constructed to tailor the polarization properties of the radiation, producing, for example, circularly polarized light. Owing to the interference effects, undulator brightness is concentrated in harmonics (first, third, fifth) and the energy of the first harmonic is typically at longer wavelengths (or lower energy) than that obtained from a wiggler (due to the lower field of the undulator). For this reason, higher energy (6–8 GeV) storage rings (i.e., APS in the United States, ESRF in France, and SPring-8 in Japan) were built in the late 1980s and early 1990s so that the useful undulator radiation could be obtained at wavelengths of around 1 Å and even much shorter. More recent advances in undulator technology, including narrow gap and in vacuum devices, have made it feasible for intermediate energy light sources (e.g., SPEAR3 at Stanford, the CLS in Canada, and Diamond in the United Kingdom with energies around 3 GeV) to achieve high X-ray brightness around 1 Å from undulators. The dramatic impact of undulators can be seen in Figure 4, where the brightness of undulator sources is on average a factor 10^4 times higher at

third-generation rings than on bending magnet sources at second-generation rings. This higher brightness enabled more challenging experiments to be conducted—pushing the boundaries to smaller crystal size, lower concentrations, faster times (for time-resolved studies), and smaller spatial resolution. Today there are approximately 50 second- and third-generation synchrotron facilities around the world, a large number of which serve active communities doing structural biology research.

There are ultimately limitations to the performance of storage rings, both in terms of brightness and the length of the electron pulses (which generate the X rays upon having their trajectories bent in bending magnets or insertion devices). Limitations on brightness come from the increase in electron beam size by the natural process of generation of synchrotron radiation. Larger circumference rings can reduce this effect, with the ultimate limit being a straight line (that is, a linear accelerator where there is no emission of synchrotron radiation to "spoil" the beam size and emittance). The nature of radio-frequency acceleration in storage rings also gives rise to a natural bunching of the electrons, which have typical bunch lengths of a few hundred picoseconds and, except for some special laser-based slicing techniques, cannot be reduced much below this value. This is illustrated graphically in Figure 4, where it can be seen to first approximation that both the second- and third-generation synchrotron sources have similar pulse lengths.

It was recognized in the 1980s and early 1990s that linacs could be interesting and revolutionary sources of synchrotron radiation. Electrons, being charged particles, can be easily manipulated; for example, they can be compressed along their direction of travel by chirping the beam in energy (that is, introducing a spread in energy from the head to the tail of the bunch) and passing the chirped beam through a magnetic compressor (which bends the particles) where the high-energy particles travel a shorter path than the low-energy ones. The properties of the electron beam in linacs are directly determined by the source. This is in contrast to a storage ring in which the beam properties result from an equilibrium process that is controlled by the lattice of magnets that control the size, divergence, and position of the electron beam. Hence, higher-brightness electron guns offer the possibility of producing much smaller, lower-emittance beams in linacs. The work on photocathodes as bright electron sources, carried out mostly at Los Alamos National Laboratory in the 1980s, provided just the type of sources needed for free electron lasers (FELs). The ability to transport and accelerate such beams was developed by the accelerator physics community in work related to a next generation of high-energy physics machines called linear colliders. The combination of linac-based light sources with high-performance insertion devices forms the basis for concepts of a next generation (the fourth) of synchrotron light sources.

One implementation of linac-based light sources is the energy recovery linac (ERL), where the remaining energy of the electron beam after it has passed through a series of undulators is recovered (69). This results in much improved operational efficiency. Such a concept operating at relatively low energies has been tested

at the Thomas Jefferson National Accelerator Facility and has been proposed as a new X-ray source at Cornell University (22). Because the properties of the electron beam are primarily determined by the electron source (a high-brightness photocathode gun), such an ERL can have much higher peak brightness with about a thousand-fold-shorter pulse length (Figure 4). Whereas ERLs operating in the X-ray regime remain in the conceptual design stage, a linac-based light source based upon a single-pass linac has recently become operational. The subpicosecond pulsed source (SPPS) at the Stanford Linear Accelerator Center (SLAC) utilizes a 28 GeV electron beam from the SLAC linear accelerator passed through a 2.5-m-long undulator to produce a 80-fsec-pulsed X-ray beam with more than 10^7 photons per pulse (see http://www-ssrl.slac.stanford.edu for details) (12). High-performance linacs combined with insertion devices offer yet another possibility to obtain even higher brightness X-ray beams. Madey (35) first described the concept of low-gain free electron lasers in the early 1970s, and the concept of operation in a high-gain limit (with single pass) was put forward somewhat later (8). Subsequently, Pellegrini (53) proposed the idea of an X-ray free electron laser that would be based upon high-energy electrons delivered by the SLAC linac and passed through a long ($\sim$100 m) undulator. Such an XFEL, which has come to be known as the Linac Coherent Light Source (LCLS), has progressed from idea to design study and into detailed engineering and design. If funded by the U.S. Department of Energy on the anticipated schedule, LCLS will produce the world's first X-ray FEL beam in 2008 (see http://www-ssrl.slac.stanford.edu/lcls). A conceptually similar project is being planned at DESY in Hamburg (the TESLA XFEL) and is expected to be operational in the 2011–2012 time frame (see http://www-hasylab.desy.de). The photon properties of the LCLS will be remarkable, as seen in Figure 4. The high gain results in an increased peak brightness over the SPPS or planned ERLs by about 10^8. The X rays produced by LCLS will be fully transversely coherent. The pulse length, initially in the range of 100–200 fs, can be shortened to below 100 fs, and with additional research and development it is expected to approach 1 fs. Such high-brightness, short-pulse, and coherent X rays have the potential to enable revolutionary experiments in biology. Such applications in extending X-ray diffraction microscopy to the imaging of single biomolecules are considered below.

OVERCOMING THE RADIATION BARRIER WITH FEMTOSECOND X-RAY PULSES

As described in the previous sections, the ultimate resolution of X-ray diffraction microscopy for biological specimens is limited by radiation damage. Although the diffraction pattern is formed by elastically scattered photons, for every elastically scattered particle there are particles that deposit significant energy in the sample and hence cause damage (25). In the case of 12 keV X rays, the dominant interaction with atoms is photoabsorption, which, for low-Z atoms (such as C, N, O), occurs

10 times more often than elastic scattering (27). The absorption of a photon leads to a string of events, initiated by ejection of a *K*-shell (inner core) photoelectron. The atom relaxes in about 2 to 10 fs, primarily by emission of an Auger electron with energy in the range of 250 to 500 eV (39). The subsequent cascade of collisional ionizations by the photoelectrons and Auger electrons deposits half the initial energy of the X-ray photon into a roughly spherical volume on the order of about 1 micron diameter (for diamond) in about 6 fs, as determined by Monte Carlo simulation (77, 79). (The cascade takes about 100 fs to fully deposit all the initial energy.) This further leads to the breaking of chemical bonds, the excitation of vibrational modes of the material in 1–10 ps (51), and, in the absence of cryogenic cooling, diffusion or mass loss of the sample (6). Empirical estimates for the maximum dose at slow exposure in cryo-protected samples, which does not cause morphological change at the 10–50 nm scale, range from 10^8 to 10^{10} Gray (24, 36, 38, 64). This dose range corresponds to incident fluences of 2 to 200 photons/Å^2 for a protein sample exposed to 12 keV X rays.

An approach to overcoming the degrading effects of radiation damage is to record the diffraction pattern in a time shorter than the time of the damage process itself. Solem et al. (65) first suggested this idea of flash imaging as a way to overcome degradation of X-ray images of living wet cells, and hydrodynamics calculations predicted that picosecond pulses could achieve about 10 nm resolution (34). These models assumed molecular thermalization processes at the 1 to 10 ps timescale and were not appropriate for modeling behavior at shorter times and higher resolution. However, a new understanding of the damage problem came with the detailed molecular dynamics analysis of Neutze et al. (52), as shown in Figure 5, which gave the first insight that atomic resolution could be possible using femtosecond pulses from an X-ray free electron laser. This work also pointed out that there is another mechanism helping to reduce the effects of damage with short pulses, namely, that using a short pulse enables injected or "containerless" samples to be flash imaged. In this case, depending on sample size (77–79), the photoelectrons and possibly some Auger electrons will escape the sample and hence not initiate the damage reactions. This effect does, however, lead to an ever more positively charged sample as the exposure progresses, which culminates in an inertia-limited Coulomb explosion that causes the eventual disintegration of the particle. The molecular dynamics calculations of Neutze et al. were based on a stochastic model of photoionization, Auger emission, and inelastic scattering. In small timesteps, the ionization state of every atom was calculated, from which the equations of motion of all atoms were solved. The results showed that at pulse durations of 50 fs, the tolerable incident fluence increases from the slow exposure value of 200 ph/Å^2 to 10^6 ph/Å^2, and to 10^7 ph/Å^2 for 5-fs pulses. At these exposures, it was estimated that atomic resolution could indeed be achieved, especially for larger objects such as a single virus capsid.

In the work of Neutze et al. (52) the photoelectrons and Auger electrons were assumed to leave the particle without further interaction, and it was noted that in actuality they would eventually be trapped. This has the effect of neutralizing the

molecule and slowing down the Coulomb explosion, at the expense of raising the temperature of free electrons in the molecule, causing a greater rate of ionization of atoms. Such effects have been considered in greater detail in two works: one with a Monte Carlo treatment of electrons interleaved with molecular dynamics steps (30), and another with a new hydrodynamic model (S.P. Hau-Riege, R.A. London & A. Szöke, manuscript submitted). The two models appear to give similar results, with the advantage that the hydrodynamic model is not limited to small (30 Å diameter) clusters of single atomic species. However, the hydrodynamic model assumes spherical symmetry and is accurate only in an average sense. In the hydrodynamic model, the free electrons and ions are treated as two separate fluids that interact through the Coulomb force and ionization processes (described by time-dependent rate equations). While it is found that early in the exposure some Auger electrons and most photoelectrons escape, the Auger electrons start becoming trapped after about <1 to 2 fs. In addition, the photoelectrons become trapped after about 10 fs if the particle is large ($\gtrsim 100$ Å diameter). Because trapped electrons lead to further unbound electrons through collisional ionization, these cascades quickly dominate the damage process. It is also found that the trapped electrons quickly relax in energy and position to form a cloud around the positive ions, leaving a neutral core and a positively charged outer shell (similar to Debye shielding). The ion motion therefore peels off from the outer shell. In the inner core there is hardly any ion motion, but the high electron temperature leads to a great amount of ionization and blurring of the electron density. This latter effect requires pulse lengths of 10 fs or less to overcome damage with pulse fluences greater than 10^6 ph/Å^2. However, these limits might be relaxed if it were possible to reconstruct atomic positions from partially ionized atoms. The damage models described above define the structure degradation that occurs at a given spatial scale and for a particular sample size, pulse fluence (or sample dose), and duration. These models do not tell us what image resolution is achievable in a final reconstruction, which requires an analysis of the particular type of diffraction experiment.

POTENTIAL OF IMAGING SINGLE PROTEIN MOLECULES

One of the current bottlenecks in structural molecular biology is the difficulty of crystallizing protein molecules. Membrane proteins pose a particular challenge in this regard, and as a result only a relatively small number of structures of this important class have been determined. There are two established techniques to determine structure without crystals: NMR and single particle imaging using cryo-electron microscopy. However, to date NMR can solve the structures of only relatively small protein molecules, and single particle imaging using cryo-electron microscopy has been limited to a resolution of $\sim$10 Å for the asymmetrical ribosome (18) and $\sim$6 to 7 Å for highly symmetrical viruses (9).

One approach, the combination of the oversampling phasing method with femtosecond X-ray pulses, may have the potential to overcome this obstacle (52, 65). To explore this hypothesis, a computer simulation has been performed for a rubisco

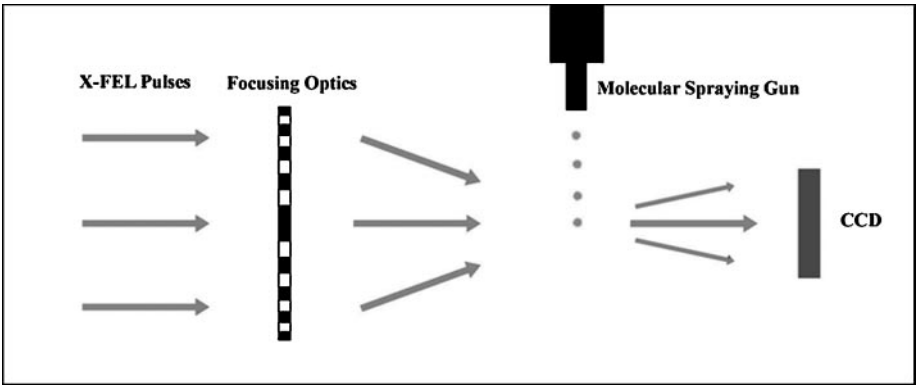

Figure 6 A possible schematic layout for the experiment of imaging single biomolecules by using X-ray free electron lasers.

protein molecule with a molecular mass of 106,392 Da (44). The atomic coordinates were obtained from the Protein Data Bank (2RUB). The rubisco molecule was "illuminated" by a simulated X-ray free electron laser with a wavelength of 1.5 Å and a pulse of 2×10^{12} photons. The pulse duration was assumed to be short enough so that radiation damage could be ignored (see Overcoming the Radiation Barrier with Femtosecond X-Ray Pulses, above). Figure 6 shows a schematic layout of a potential experimental set-up. The simulated X-ray laser was focused down to a 0.1 μm spot, for a pulse fluence of 2.55×10^6 ph/Å^2. The molecules were "dropped" into the beam in random orientation one at a time by a molecular spraying gun. In the simulation, each molecule was assumed to be hit by an X-ray pulse, and a total of 10^6 two-dimensional diffraction patterns were obtained from the identical rubisco molecules. The oversampled two-dimensional diffraction patterns were assembled to an oversampled three-dimensional diffraction pattern (160^3 voxels) with the assumption that the orientation of each molecule (and hence the two-dimensional diffraction pattern) was known. To simulate a beamstop, the data in the central $3 \times 3 \times 3$ voxels were removed. Poisson noise was then added to the molecule transform with $R = 9.7\%$, where the R factor was used to characterize the difference between the noise-free molecule transform and the noisy one. By using the oversampling phasing method, the phasing information was ab initio retrieved from the three-dimensional diffraction pattern. Figure 7*b* shows the reconstructed electron density map of the active site, which is in a good agreement with the same map obtained from the Protein Data Bank (Figure 7*a*). To study the effect of noise on the quality of the reconstruction, higher Poisson noise was added to the three-dimensional diffraction pattern with $R = 16.6\%$, where 3×10^5 identical molecules were used for the calculation. Figure 7*c* shows the reconstructed three-dimensional electron density of the active site.

Although the computer simulation demonstrated the potential of imaging single molecules by combining the oversampling method with femtosecond X-ray pulses, it made two favorable assumptions: (*a*) Radiation damage can be circumvented by

using femtosecond X-ray pulses and (*b*) the molecular orientation can be precisely determined. So far the computer modeling seems to support the first assumption (see Overcoming the Radiation Barrier with Femtosecond X-Ray Pulses, above), and a real test has to wait for the availability of X-ray free electron lasers. The determination of molecular orientation could be carried out by two methods. One is to determine the molecular orientation from a series of two-dimensional diffraction patterns, which has already been developed in single particle imaging using cryo-electron microscopy (14, 18). The other is to use a laser field to physically align each molecule before the exposure (32). With regard to the first method, a detailed statistical analysis that determines the signal levels required to classify diffraction patterns of randomly oriented particles has been performed (28). At the highest resolution, where the signal is weakest and the orientation determination is the most stringent, classification can be performed with signal levels below one photon per pixel. In general, for a given incident intensity and desired resolution, patterns from larger particles are easier to classify not only because they scatter more, but because there are more independent pixels on which to perform the correlation. At fluences of 2×10^6 ph/Å^2 it is possible to classify patterns of 100 Å diameter molecules at a resolution better than 3 Å. At this intensity, as was discussed in the previous section, it should be possible to record diffraction patterns to this resolution with ∼10-fs pulses.

SUMMARY AND OUTLOOK

X-ray diffraction microscopy, a combination of coherent and bright X rays with the oversampling phasing method, is a newly developed methodology that promises to make it possible to escape the "benevolent tyranny" of the crystal in the reconstruction of structure from diffraction data (29). Due to the loss of the amplification from a large number of unit cells inside crystals, the major limitation of the application to structural biology seems to be radiation damage. By using cryo technologies, radiation damage can be significantly reduced, which makes it possible to image cells and cellular structures with X-ray diffraction microscopy. If with the planned femtosecond-pulsed X-ray lasers a two-dimensional diffraction pattern could be recorded from a biomolecule before it is destroyed, this technique could open a new horizon of imaging macromolecules without the need to first crystallize them.

ACKNOWLEDGMENTS

We gratefully acknowledge our respective collaborators, including T. Ishikawa, Y. Nishino, C. Larabell, M. LeGros, D. Durkin, T. Beetz, C. Jacobsen, E. Lima, D. Shapiro, S. Hau-Riege, R. London, A. Szöke, S. Marchesini, A. Noy, M. Howells, J. Spence, H. He, J. Hajdu, and G. Huldt. This work was supported by the U.S. Department of Energy, Office of Basic Energy Sciences. Additional support was provided by the U.S. Department of Energy Office of Biological and Environmental Research and the National Institutes of Health. Part of this work

was performed under the auspices of the U.S. Department of Energy by University of California, Lawrence Livermore National Laboratory, under Contract No. W-7405-ENG-48. Use of the RIKEN beamline (BL29XUL) at SPring-8 was supported by RIKEN.

The *Annual Review of Biophysics and Biomolecular Structure* is online at http://biophys.annualreviews.org

LITERATURE CITED

1. Argos P, Rossmann MG. 1980. Molecular replacement method. In *Theory and Practice of Direct Methods in Crystallography*, ed. MFC Ladd, RA Palmer, pp. 361–417. New York: Plenum
2. Barakat R, Newsam G. 1984. Necessary conditions for a unique solution to two-dimensional phase recover. *J. Math. Phys.* 25:3190–93
3. Barletta WA, Winick H. 2003. Introduction to special section on future light sources. *Nucl. Instr. Methods A* 500:1–10
4. Bates RHT. 1982. Fourier phase problems are uniquely soluble in more than one dimension. I. Underlying theory. *Optik* 61:247–62
5. Baumeister W, Grimm R, Walz J. 1999. Electron tomography of molecules and cells. *Trends Cell Biol.* 9:81–85
6. Beetz T, Jacobsen C. 2002. Soft X-ray radiation damage studies in PMMA using a cryo-STXM. *J. Synchrotron Radiat.* 10:280–83
7. Beetz T, Jacobsen C, Kao CC, Kirz J, Mentes O, et al. 2003. Development of novel apparatus for experiments in soft X-ray diffraction imaging and diffraction tomography. *J. Phys. IV Fr.* 104:27–30
8. Bonifacio R, Pellegrini C, Narducci LM. 1984. Collective instabilities and high gain regime in a free-electron laser. *Opt. Commun.* 50:373–78
9. Bottcher B, Wynne SA, Crowther RA. 1997. Determination of the fold of the core protein of hepatitis B virus by electron cryomicroscopy. *Nature* 386:88–91
10. Bricogne G. 1974. Geometric sources of redundancy in intensity data and their use for phase determination. *Acta Crystallogr. A* 30:395–405
11. Bruck YM, Sodin LG. 1979. On the ambiguity of the image reconstruction problem. *Opt. Commun.* 30:304–8
12. Cornacchia M, Arthur J, Bentson L, Carr R, Emma P, et al. 2001. Sub-picosecond photon pulse facility for SLAC. *SLAC-PUB-8950*
13. Crowther RA. 1969. The use of non-crystallographic symmetry for phase determination. *Acta Crystallogr. B* 25:2571–80
14. Crowther RA. 1971. Procedures for three-dimensional reconstruction of spherical viruses by Fourier synthesis from electron micrographs. *Philos. Trans. R. Soc. London Ser. B.* 261:221–30
15. Elser V. 2003. Phase retrieval by iterated projections. *J. Opt. Soc. Am. A* 20:40–55
16. Fienup JR. 1978. Reconstruction of an object from the modulus of its Fourier transform. *Opt. Lett.* 3:27–29
17. Fienup JR. 1987. Reconstruction of a complex-valued object from the modulus of its Fourier transform using a support constraint. *J. Opt. Soc. Am. A* 4:118–23
18. Frank J. 2002. Single-particle imaging of macromolecules by cryo-electron microscopy. *Annu. Rev. Biophys. Biomol. Struct.* 31:303–19
19. Gerchberg RW, Saxton WO. 1972. A practical algorithm for the determination of phase from image and diffraction plane pictures. *Optik* 35:237–46
20. Giacovazzo C. 1998. *Direct Phasing in*

Crystallography. New York: Oxford Univ. Press
21. Green DW, Ingram VM, Perutz MF. 1954. The structure of haemoglobin. IV. Sign determination by the isomorphous replacement method. *Proc. R. Soc. London Ser. A* 255:287–307
22. Gruner SM, Tigner M. 2001. Study for a proposed Phase I energy recovery linac (ERL) synchrotron light source at Cornell University. *CHESS Tech. MEMO 01-003* and *JLAB-ACT-01-04*
23. He H, Marchesini S, Howells M, Weierstall U, Chapman H, et al. 2003. Inversion of X-ray diffuse scattering to images using prepared objects. *Phys. Rev. B* 67:174114
24. Henderson R. 1990. Cryoprotection of protein crystals against radiation damage in electron and X-ray diffraction. *Proc. R. Soc. London Sci. Ser. B* 241:6–8
25. Henderson R. 1995. The potential and limitations for neutrons, electrons and X-rays for atomic resolution microscopy of unstained biological molecules. *Q. Rev. Biophys.* 28:171–93
26. Hendrickson WA, Smith JL, Sheriff S. 1985. Direct phase determination based on anomalous scattering. *Methods Enzymol.* 115:41–55
27. Henke BL, Gullikson EM, Davis JC. 1993. X-ray interactions: photoabsorption, scattering, transmission, and reflection at E = 50–30000 eV, Z = 1–92. *At. Data Nucl. Data Tables* 54:181–342
28. Huldt G, Szöke A, Hajdu J. 2003. Diffraction imaging of single particles and biomolecules. *J. Struct. Biol.* 144:219–27
29. Johnson LN, Blundell TL. 1999. Introductory overview. *J. Synchrotron Radiat.* 6:813–15
30. Jurek Z, Faigel G, Tegze M. 2003. Dynamics in a cluster under the influence of intense femtosecond hard X-ray pulses. http://arxiv.org/abs/physics/0306102
31. Kirz J, Jacobsen C, Howells M. 1995. Soft X-ray microscopes and their biological applications. *Q. Rev. Biophys.* 28:33–130
32. Larsen JJ, Hald K, Bjerre N, Stapelfeldt H, Seideman T. 2000. Three-dimensional alignment of molecules using elliptically polarized laser fields. *Phys. Rev. Lett.* 85: 2470–73
33. Lima E, Shapiro D, Kirz J, Sayre D. 2003. Algorithmic image reconstruction using iterative phase retrieval schema. *J. Phys. IV Fr.* 104:631–34
34. London RA, Rosen MD, Trebes JE. 1989. Wavelength choice for soft X-ray laser holography of biological samples. *Appl. Opt.* 28:3397–404
35. Madey JM. 1971. Stimulated emission of Bremsstrahlung in a periodic magnetic field. *J. Appl. Phys.* 42:1906
36. Marchesini S, Chapman HN, Hau-Riege SP, London RA, Szöke A, et al. 2003. Coherent X-ray diffractive imaging: applications and limitations. *Opt. Exp.* 11:2344–53
37. Marchesini S, He H, Chapman HN, Hau-Riege SP, Noy A, et al. 2003. X-ray imaging without lenses. *Phys. Rev. B.* In press
38. Maser J, Osanna A, Wang Y, Jacobsen C, Kirz J, et al. 2000. Soft X-ray microscopy with a cryo STXM. I. Instrumentation, imaging, and spectroscopy *J. Microsc.* 197:68–79
39. McGuire EJ. 1969. K-shell Auger transition rates and fluorescence yields for elements Be-Ar. *Phys. Rev.* 185:1–6
40. McIntosh JR. 2001. Electron microscopy of cells: a new beginning for a new century. *J. Cell Biol.* 153:25–32
41. Miao J, Amonette JE, Nishino Y, Ishikawa T, Hodgson KO. 2003. Direct determination of the absolute electron density of nanostructured and disordered materials at sub-10-nm resolution. *Phys. Rev. B* 68:012201
42. Miao J, Charalambous P, Kirz J, Sayre D. 1999. Extending the methodology of X-ray crystallography to allow imaging of micrometer-sized non-crystalline specimens. *Nature* 400:342–44
43. Miao J, Hodgson KO, Ishikawa T, Larabell CA, LeGros MA, Nishino Y. 2003. Imaging whole Escherichia coli bacteria by

using single-particle X-ray diffraction. *Proc. Natl. Acad. Sci. USA* 100:110–12
44. Miao J, Hodgson KO, Sayre D. 2001. An approach to three-dimensional structures of biomolecules by using single-molecule diffraction images. *Proc. Natl. Acad. Sci. USA* 98:6641–45
45. Miao J, Ishikawa T, Anderson EH, Hodgson KO. 2003. Phase retrieval of diffraction patterns from non-crystalline samples by using the oversampling method. *Phys. Rev. B* 67:174104
46. Miao J, Ishikawa T, Johnson B, Anderson EH, Lai B, Hodgson KO. 2002. High resolution three-dimensional X-ray diffraction microscopy. *Phys. Rev. Lett.* 89:088303
47. Miao J, Kirz J, Sayre D. 2000. The oversampling phasing method. *Acta Crystallogr. D* 56:1312–15
48. Miao J, Sayre D. 2000. On possible extensions of X-ray crystallography through diffraction-pattern oversampling. *Acta Crystallogr. A* 56:596–605
49. Miao J, Sayre D, Chapman HN. 1998. Phase retrieval from the magnitude of the Fourier transforms of non-periodic objects. *J. Opt. Soc. Am. A* 15:1662–69
50. Millane RP. 1996. Multidimensional phase problems. *J. Opt. Soc. Am. A* 13:725–34
51. Mozumder A. 1969. Charged particle tracks and their structure. In *Advances in Radiation Chemistry*, ed. M Burton and JL Magee, pp. 1–102. New York: Wiley
52. Neutze R, Wouts R, Spoel D, Weckert E, Hajdu J. 2000. Potential for biomolecular imaging with femtosecond X-ray pulses. *Nature* 406:752–57
53. Pellegrini C. 1992. A 4 to 0.1 FEL based on the SLAC Linac. In *Proceedings of the Workshop on 4th Generation Light Sources*, ed. M Cornacchia, H Winick, pp. 376–84. Stanford, CA: SLAC
54. Phillips JC, Wlodawer A, Goodfellow JM, Watenpaugh KD, Sieker LC, et al. 1977. Applications of synchrotron radiation to protein crystallography. II. Anomalous scattering, absolute intensity, and polarization. *Acta Crystallogr. A* 33:445–55
55. Phillips JC, Wlodawer A, Yevitz MM, Hodgson KO. 1976. Applications of synchrotron radiation to protein crystallography: preliminary results. *Proc. Natl. Acad. Sci. USA* 73:128–32
56. Robinson IK, Vartanyants IA, Williams GJ, Pfeifer MA, Pitney JA. 2001. Reconstruction of the shapes of gold nanocrystals using coherent X-ray diffraction. *Phys. Rev. Lett.* 87:195505
57. Rossmann MG, Blow DM. 1963. Determination of phases by the conditions of noncrystallographic symmetry. *Acta Crystallogr.* 16:39–45
58. Sayre D. 1952. Implications of a theorem due to Shannon. *Acta Crystallogr.* 5:843
59. Sayre D. 1980. Prospects for long-wavelength X-ray microscopy and diffraction. In *Imaging Processes and Coherence in Physics. Springer Lecture Notes in Physics*, Vol. 112, ed. M Schlenker, M Fink, JP Goedgebuer, C Malgrange, JC Vienot, RH Wade, pp. 229–35. Berlin: Springer
60. Sayre D. 1991. Note on "superlarge" structures and their phase problem. In *Direct Methods of Solving Crystal Structures*, ed. H Schenck, pp. 353–56. New York: Plenum
61. Sayre D, Chapman H. 1995. X-ray microscopy. *Acta Crystallogr. A* 51:237–52
62. Sayre D, Chapman HN, Miao J. 1998. On the extendibility of X-ray crystallography to noncrystals. *Acta Crystallogr. A* 54:233–39
63. Sayre D, Kirz J, Feder R, Kim DM, Spiller E. 1977. Transmission microscopy of unmodified biological materials: comparative radiation dosages with electrons and ultrasoft X-ray photons. *Ultramicroscopy* 2:337–41
64. Schneider G. 1998. Cryo X-ray microscopy with high spatial resolution in amplitude and phase contrast. *Ultramicroscopy* 75:85–104
65. Solem J, Baldwin GC. 1982. Microholography of living organisms. *Science* 218:229–35
66. Spence JCH, Howells M, Marks LD, Miao J. 2001. Lensless imaging: a workshop

on new approaches to the phase problem for non-periodic objects. *Ultramicroscopy* 90:1–6
67. Spence JCH, Wu JS, Giacovazzo C, Carrozzini B, Cascarano GL, Padmore HA. 2003. Solving non-periodic structures using direct methods: phasing diffuse scattering. *Acta Crystallogr. A* 59:255–61
68. Stroud RM, Agard DA. 1979. Structure determination of asymmetric membrane profiles using an iterative Fourier method. *Biophys. J.* 25:495–512
69. Tigner M. 1965. A possible apparatus for electron clashing-beam experiments. *Nuovo Cimento* 37:1228–31
70. Vartanyants IA, Robinson IK. 2001. Partial coherence effects on the imaging of small crystals using coherent X-ray diffraction. *J. Phys. Condens. Matter* 13:10593–611
71. Wang BC. 1985. Resolution of phase ambiguity in macromolecular crystallography. *Methods Enzymol.* 115:90–112
72. Watenpaugh K, Smith J, eds. 1991. *Report of the Biological Synchrotron Users Organization* (*Biosync*). http://biosync.sdsc.edu/
73. Weierstall U, Chen Q, Spence JCH, Howells MR, Isaacson M, Panepucci RR. 2001. Image reconstruction from electron and X-ray diffraction patterns using iterative algorithms: experiment and simulation. *Ultramicroscopy* 90:171–95
74. Williams GJ, Pfeifer MA, Vartanyants IA, Robinson IK. 2003. Three-dimensional imaging of microstructure in Au nanocrystals. *Phys. Rev. Lett.* 90:175501
75. Woolfson M, Fan HF. 1995. *Physical and Non-physical Methods of Solving Crystal Structures.* Cambridge: Cambridge Univ. Press
76. Yun W, Kirz J, Sayre D. 1987. Observation of the soft X-ray diffraction pattern of a single diatom. *Acta Crystallogr. A* 43:131–33
77. Ziaja B, Szöke A, Hajdu J. 2002. Electron cascades produced by photoelectrons in diamond. http://arxiv.org/abs/cond-mat/0208515
78. Ziaja B, Szöke A, van der Spoel D, Hajdu J. 2002. Space-time evolution of electron cascades in diamond. *Phys. Rev. B* 66:024116
79. Ziaja B, van der Spoel D, Szöke A, Hajdu J. 2001. Auger-electron cascades in diamond and amorphous carbon. *Phys. Rev. B* 64:214104

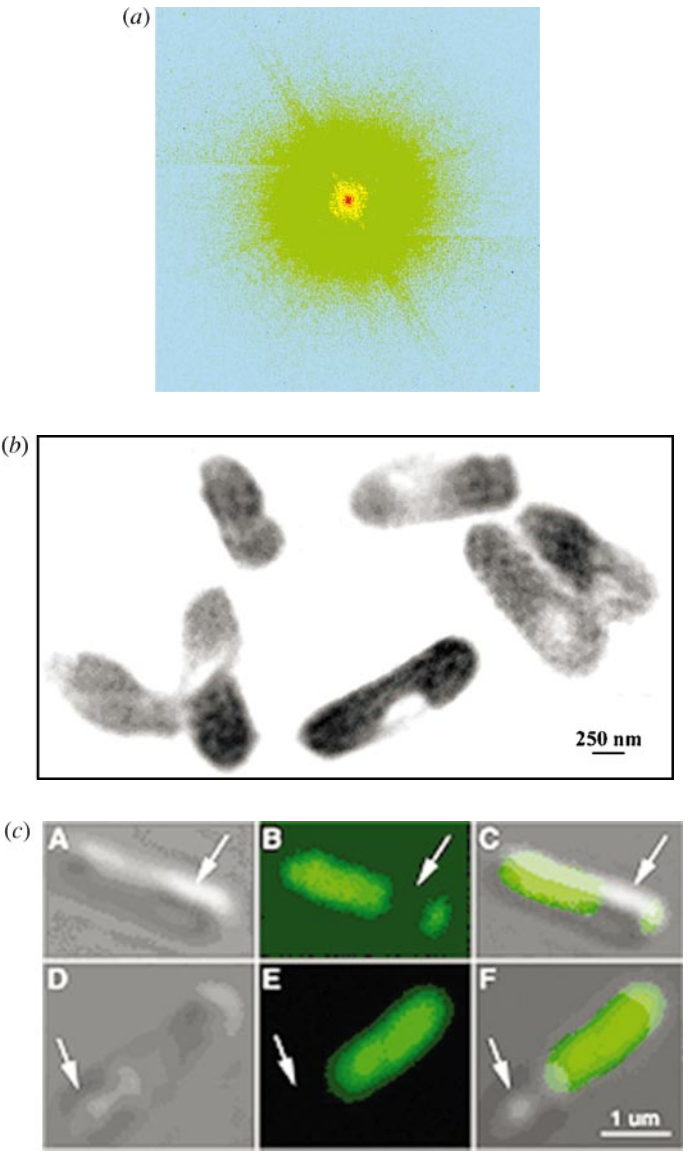

Figure 2 (*a*) An oversampled X-ray diffraction pattern from *E. coli* bacteria. (*b*) An image reconstructed from (*a*). The dense regions inside the bacteria are likely the distribution of proteins labeled with $KMnO_4$. The semitransparent regions are devoid of yellow fluorescence proteins, which are consistent with (*c*). (*c*) *E. coli* expressing the indicator protein. Individual bacteria are seen using transmitted light (A, D) and fluorescence (B, E), where the yellow fluorescence protein (*green*) is seen throughout most of the bacteria except for one small region in each bacterium that is free of fluorescence (*arrows*). C and F show the fluorescent image superimposed on the transmitted light image. See Reference 43 for details.

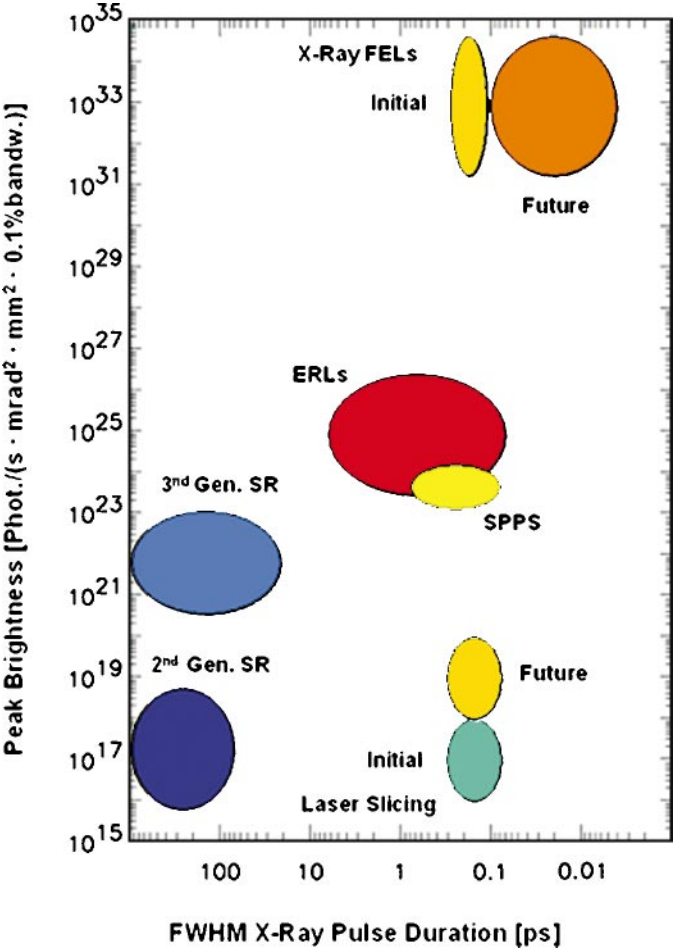

Figure 4 Peak brightness and X-ray pulse duration for a general class of second- and third-generation storage rings compared with that made possible from a next generation of linac-based sources. Also shown is a special type of "sliced" storage ring source, an example of which has recently become operational at the ALS in Berkeley. The ERLs/SPPS and XFELs offer the possibility of dramatic increases in per pulse brightness combined with much shorter pulse duration. The original concept for such a plot was given in conjunction with the Cornell proposal for an ERL (see Reference 22) and further elaborated in Reference 3. XFELs with high peak brightness and short pulse duration are required for imaging single biomolecules. The latest generation of storage rings, and especially ERLs can be optimized to provide high time-averaged coherent flux, and are best suited for three-dimensional imaging of cells and other objects where identical copies are not available.

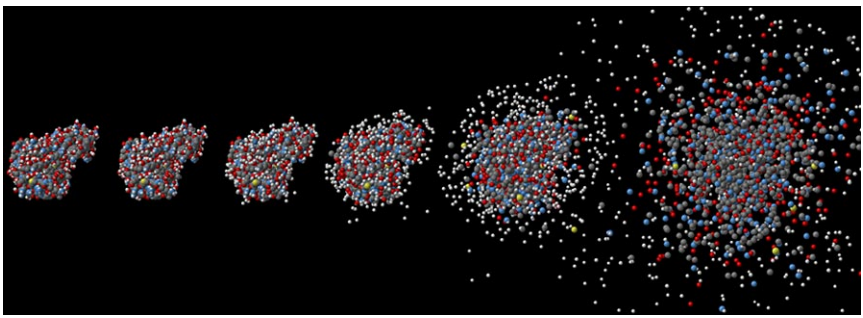

Figure 5 Results of molecular dynamics simulations of the interaction of a T4 lysozyme molecule with an XFEL pulse, for a pulse fluence of $3.8 * 10^6$ ph/A^2, and 2 fs duration (FWHM). The sequence of pictures shows atom positions at 2 fs before the peak of the pulse, and then 2, 5, 10, 20, and 50 fs after the peak of the pulse. The Coulomb explosion of the molecule is clearly seen and does not occur until after the pulse exposure. The atomic positions of the structure remain practically the same throughout the duration of the pulse because of the inertial delay of the explosion. However, ionization has occurred, which changes the scattering factors and hence changes the diffraction pattern, such that the time-integrated pattern differs from the ideal by an R factor of 11%. Reproduced from Reference 52.

(*a*)

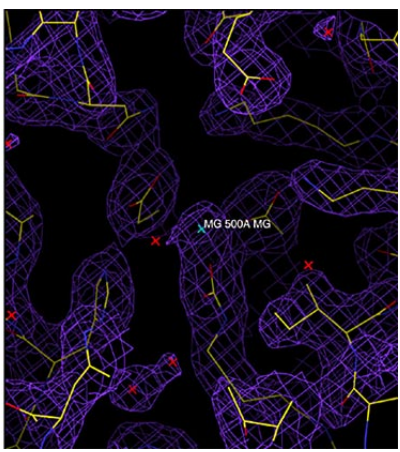

Figure 7 Structural determination of single rubisco molecules utilizing a simulated XFEL and direct phase retrieval by the oversampling method. (*a*) Stereoview of the electron density map of the active site with a Mg(II) of the rubisco molecule (contoured at two sigma), on which the refined atomic model of the rubisco molecule is superimposed. The electron density map and the atomic model are obtained from Protein Data Bank. (*b*) The active site reconstructed from a three-dimensional diffraction pattern with R = 9.7%, on which the same atomic model is superimposed. (*c*) The reconstructed active site with R = 16.6%. (See Reference 44 for details.)

(*b*)

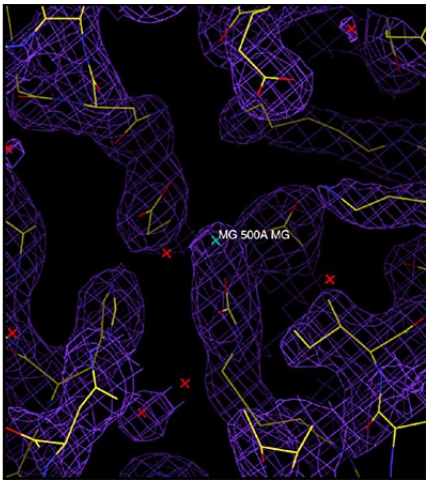

(*c*)

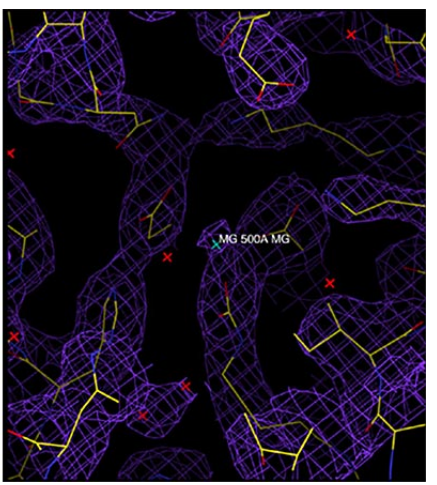

Figure 7 (*Continued***)**